Densely arrayed cage-shaped polymer topologies synthesized via cyclopolymerization of star-shaped macromonomers

Yoshinobu Mato,[†] Maho Sudo,[†] Hironori Marubayashi,[§] Brian J. Ree,[‡] Kenji Tajima,[‡] Takuya Yamamoto,[‡] Hiroshi Jinnai,[§] Takuya Isono,[‡,] Toshifumi Satoh[‡,*]*

[†]Graduate School of Chemical Sciences and Engineering, Hokkaido University, Sapporo 060-8628, Japan

[‡]Division of Applied Chemistry, Faculty of Engineering, Hokkaido University, Sapporo 060-8628, Japan

[§]Institute of Multidisciplinary Research for Advanced Materials, Tohoku University, 2-1-1 Katahira, Aoba-ku, Sendai, Miyagi 980-8577, Japan

For Table of Contents Use Only

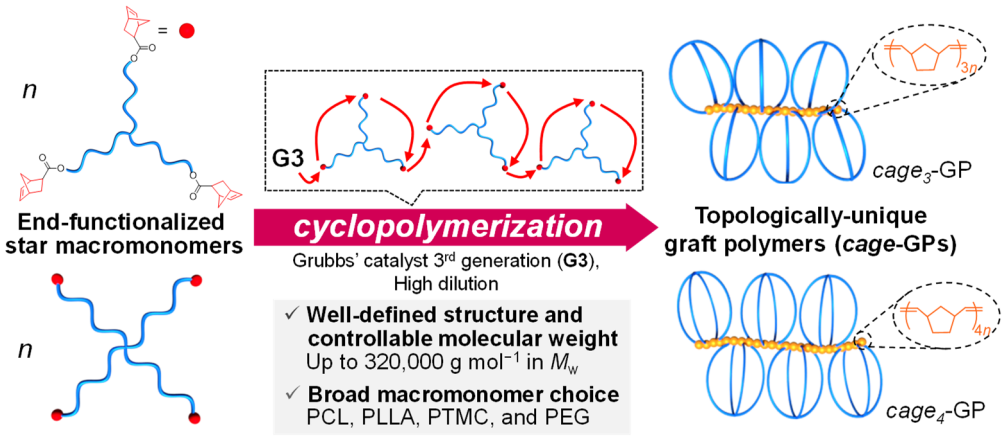

ABSTRACT: This work reports a facile and versatile ring-opening metathesis polymerization of three- and four-armed star-shaped poly(ε-caprolactone) (PCL) macromonomers bearing a norbornenyl group at each chain-end using diluted Grubbs' third-generation catalyst to obtain graft polymers (GPs) comprising densely arrayed three- and four-armed cage-shaped grafted PCLs (GPCLs) with narrow dispersity (1.19–1.35) and controllable number of cage repeating units up to 40 (molecular weight: ~320,000 g mol^{-1}). The GPCLs were characterized using nuclear magnetic resonance spectroscopy, size exclusion chromatography, and matrix-assisted laser desorption/ionization-time of flight mass spectrometry. The cyclopolymerization proceeded via repetitive rapid intramolecular reactions to form cage-shaped units followed by slow intermolecular propagation. This synthesis was applicable to star-shaped poly(L-lactide), poly(trimethylene carbonate), and poly(ethylene glycol). Investigating the structure–property relationships between crystallization behavior, hydrodynamic diameter, and viscosity revealed that cage-shaped topological side-chains reduced the chain dimensions and mobility compared to their linear and cyclic counterparts.

Introduction

Polymer chain topology is one of the important structural variables for designing polymeric materials possessing sophisticated functions.[1] The cyclic topology has attracted particular interest owing to its higher density,[2] smaller hydrodynamic volume,[3] and superior optical properties[4] compared to its linear counterparts having the same composition and molecular weight, which stems from the lack of chain-ends. Advances in polymer chemistry have made it possible to synthesize not only monocyclic polymers but also polymers possessing complicated cyclic topologies. Consequently, experimental and theoretical studies on how these intriguing topologies affect the properties and functions of the polymers have recently attracted considerable interest.[5–8]

As a result, significant efforts have been devoted to the development of functional materials and interfaces by integrating cyclic polymer chains. Examples include viscoelastically augmented gels prepared by chemical crosslinking of a cyclic polymer[9] and thermostable micelles formed by the self-assembly of cyclic block copolymers.[10] Cyclic-chain grafting onto diverse surfaces or interfaces, such as bulk metals,[11–14] metal nanoparticles,[15,16] and damaged cartilage[17,18], have been discovered as highly efficient means to improve the colloidal stability of metallic nanoparticles and enhance the bioinertness and lubricating properties of biomaterials. The Benetti group has demonstrated that graft polymers (i.e., bottlebrush polymer) fabricated using macrocyclic poly(2-alkyl-2-oxazoline) side-chains can be used as surface modifiers to impart biomaterials with superior lubricating abilities and antifouling natures.[19] These intriguing properties arise from the suppressed chain entanglement in cyclic polymers, which is

further enhanced by the denser packing of the polymer chains due to the graft-polymer-like architecture. Therefore, it is of particular interest to synthesize unique graft polymers (GPs) carrying various cyclic topological polymer side-chains possessing tunable grafting densities, which could further expand their potential applications as surface modifiers. The cage-shaped topology is particularly interesting for functional surface/interface applications because of its diminished chain entanglement and molecular dimensions compared to its monocyclic counterparts. In addition, the three-dimensional structure of the cage-shaped framework may serve as a platform for novel supramolecular nanomaterial applications, as inspired by cryptands.[20] Therefore, graft polymers with densely arrayed cage-shaped side-chains (*cage*-GPs, Figure 1) are intriguing synthetic targets.

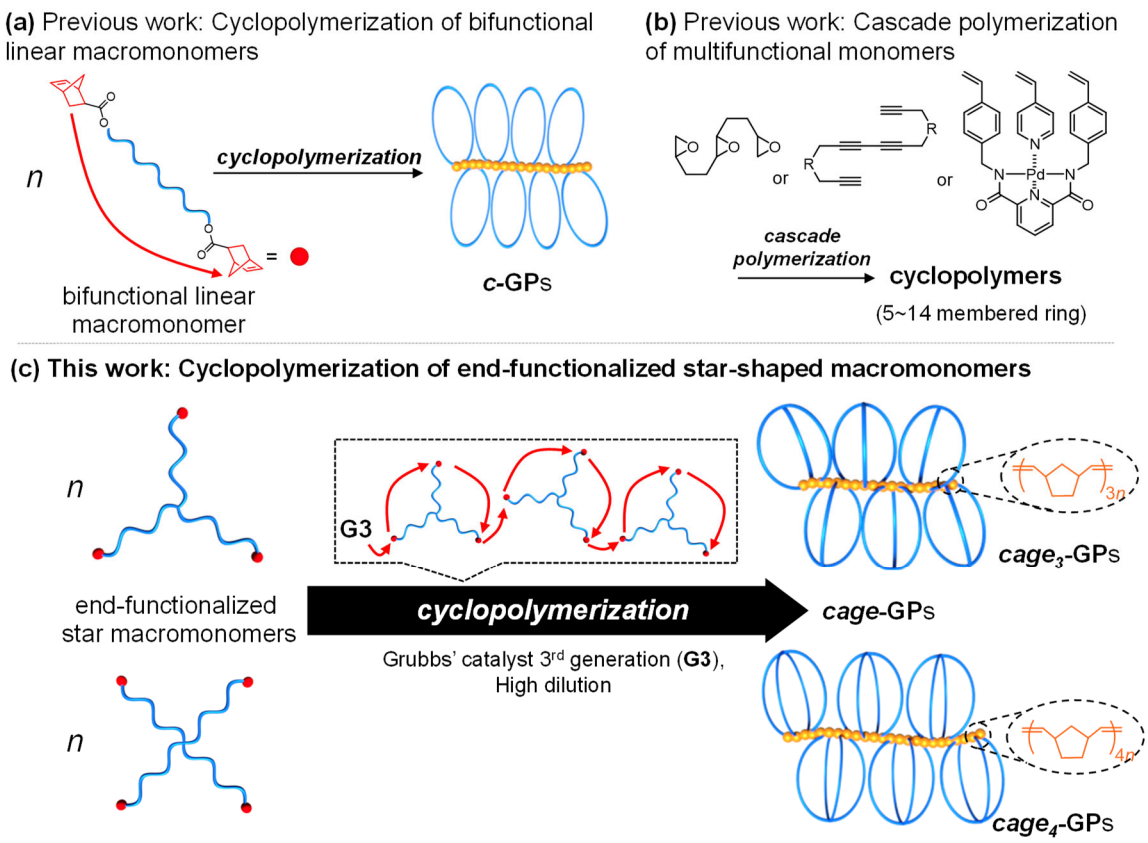

Figure 1. Schematic of cyclopolymerization strategies for constructing architecturally unique polymers. (a) Cyclopolymerization of linear bifunctional macromonomers to produce cyclic GPs (*c*-GPs). (b) Cascade polymerization of multifunctional monomers to produce corresponding cyclopolymers having small rings. (c) Cyclopolymerization of norbornenyl-end-functionalized star-shaped macromonomers to synthesize *cage*-GPs.

Generally, graft polymers can be synthesized by three different methods[21]: (i) grafting from, (ii) grafting onto, and (iii) grafting through. Approach (i) is applicable solely to the synthesis of graft polymers possessing linear side-chains and is therefore impossible to apply to *cage*-GP synthesis. Approach (ii) may be applied to the construction of *cage*-GPs by grafting a separately prepared cage-shaped macromolecule onto a reactive polymer backbone. This is probably feasible because some researchers have reported the synthesis of GPs possessing monocyclic side-chains (*c*-GPs) by the grafting onto method.[19,22–24] However, the necessity of preparing cage-shaped macromolecules

containing a reactive functional group is a major hurdle in the way of realizing this approach. Furthermore, this strategy inherently produces poorly-defined *cage*-GPs because the quantitative grafting of bulky polymeric chains is challenging. Approach (iii) is advantageous over the other two approaches in its ability to precisely construct well-defined *cage*-GPs. However, this approach also requires the preparation of cage-shaped macromonomers.

We recently established a robust synthetic pathway to *c*-GPs without using cyclic macromonomers. The cyclopolymerization of *α*,*ω*-norbornenyl-functionalized bifunctional linear macromonomers produces well-defined multicyclic polymers through ring-opening metathesis polymerization (ROMP) using Grubbs' third generation catalyst (G3) (Figure 1a).[25,26] The cyclopolymerization is facilitated by the significantly quicker intramolecular cyclization compared to the intermolecular propagation under highly diluted conditions. We envisioned that extending this approach would directly yield the corresponding *cage*-GPs from star-shaped macromonomers containing polymerizable groups at each chain-end. A few examples of the cascade cyclopolymerization of specially designed multifunctional monomers (e.g., trivinyl,[27] tetrayne,[28] and triepoxide[29]) have been reported previously (Figure 1b). However, such multifunctional monomers all have a low molecular degree of freedom. Consequently, they exclusively produce small-ringed cyclopolymers (up to 14-membered rings[27]). Therefore, the establishment of the cyclopolymerization of star-shaped macromonomers to construct a large topological unit is of significant fundamental interest. Furthermore, generating mechanistic insights into cyclopolymerization may provide elementary yet crucial knowledge to expand the ROMP-based

syntheses of a variety of architecturally complex macromolecules. Herein, we report a facile and versatile synthesis of graft polymers carrying three- and four-armed cage-shaped polymer side-chains through the cyclopolymerization of three- and four-armed star-shaped macromonomers, respectively, that bear a norbornenyl group at each chain-end (Figure 1c). As a model polymer, poly(ε-caprolactone) (PCL) was employed due to its ease of preparation using diphenyl phosphate as a catalyst with sufficient chain-end fidelity and narrow dispersity ($Đ < 1.1$).[30] Employing this synthetic approach, we have successfully synthesized a series of *cage*-GPs containing different numbers of cage-shaped grafted PCL units (*cage*-GPCLs), together with GPCLs containing linear and cyclic side-chains as reference samples, which facilitated a systematic study on the structure-property relationships (i.e., melting temperature, crystallinity, viscosity, and hydrodynamic diameter) of topological GPCLs in the bulk as well as solution states. Additionally, the versatility of the proposed synthetic approach was further confirmed by applying it to other macromonomers consisting of poly(trimethylene carbonate), polylactide, and poly(ethylene oxide).

Results and Discussion

Cyclopolymerization of three-armed star-shaped macromonomer. To produce the GPCL with three-armed cage-shaped side-chains (*cage*$_3$-GPCL), we initially prepared a three-armed star-shaped macromonomer (*s*-(PCL-NB)$_3$; number-average molecular weight (M_n) estimated by proton nuclear magnetic resonance spectroscopy (^{1}H NMR) ($M_{n,NMR}$) = 5200 g mol^{-1}, M_n estimated by size exclusion chromatography (SEC) equipped with a refractive index detector using PSt standards ($M_{n,SEC}$) = 8000 g mol^{-1}, $Đ$ = 1.10) following the procedure reported in our previous paper (Scheme 1a).[31] Note that each PCL arm of the macromonomers was designed to have a number-average molecular weight of approximately 1500 g mol^{-1} throughout this paper regardless of the number of arms. Also, the perfect functionality (>99%) of end-norbornenyl group in the star macromonomer was ensured by ^{1}H NMR analysis (Figure S1), by which the signal due to the methylene adjacent to the hydroxy end group (3.6 ppm) completely disappeared after the treatment with *exo*-5-norbornene carboxylic acid. Subsequently, the cyclopolymerization of *s*-(PCL-NB)$_3$ was performed in CH_2Cl_2 by adding G3 stock solution to the macromonomer solution at a $[s\text{-(PCL-NB)}_3]_0/[G3]_0$ = 5/1 (Table 1; see SI for synthetic details). Assuming the living polymerization nature of G3-mediated ROMP,[26] this should produce a GPCL containing five cage units on average if the cyclopolymerization proceeds in an accurately controlled manner. To realize an accurately controlled cyclopolymerization system, it is necessary to find an optimized reaction condition in which intramolecular cyclization takes place significantly more rapidly than intermolecular propagation. An insufficient difference in the reaction rates of the two elementary

competitive reactions causes dangling chain formation, which in turn induces intermolecular crosslinking, finally leading to gelation. We initially examined the effect of macromonomer concentration ($[s\text{-(PCL-NB)}_3]_0$). At $[s\text{-(PCL-NB)}_3]_0$ = 5.0 mM, gelation occurred upon the addition of the G3 solution, suggesting competition between the intramolecular cyclization and intermolecular propagation, leading to significant intermolecular crosslinking. To selectively promote the intramolecular cyclization, the macromonomer was diluted further ($[s\text{-(PCL-NB)}_3]_0$ = 1.0 and 0.1 mM). Even at $[s\text{-(PCL-NB)}_3]_0$ = 1.0 mM, SEC analysis revealed a broad multimodal peak over the high-molecular region at a polymerization time of 30 min, and continuing the polymerization resulted in an insoluble product (Figure S2). In contrast, the reaction at $[s\text{-(PCL-NB)}_3]_0$ = 0.1 mM produced a soluble product. The SEC trace of the product clearly shifted to a higher molecular region ($M_{n,SEC}$ = 26200 g mol^{-1}, $Đ$ = 1.20) compared to that of the macromonomer ($M_{n,SEC}$ = 8000 g mol^{-1}, $Đ$ = 1.10), while retaining the monomodal peak shape (Figure 2a). This indicated that the intramolecular cyclization proceeded much more rapidly than intermolecular propagation under such highly diluted conditions.

Scheme 1. Synthesis of topological graft PCLs containing (a) three- and (b) four-armed cage-shaped side-chains via the cyclopolymerizations of the corresponding star-shaped PCLs containing a norbornenyl group at each chain-end.

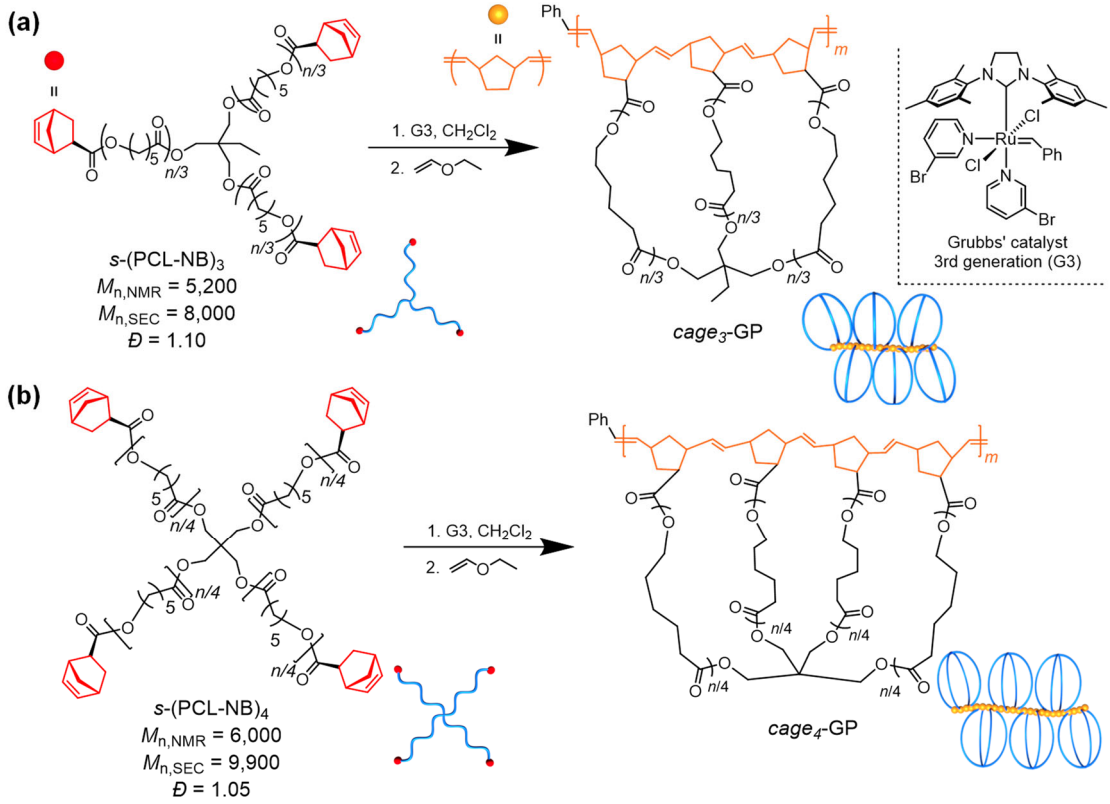

Table 1. Molecular characterization of graft polymers containing *cage*$_x$-shaped (x = 3 and 4) side-chains (*cage*$_x$-GPCLs (x = 3 and 4), respectively)[a]

Sample	MM	$[MM]_0/[G3]_0$	$[MM]_0$ (mol L^{-1})	time (min)	$M_{n,SEC}$ [b] (g mol^{-1})	$M_{n,MALS}$ [c] (g mol^{-1})	$Đ$ [b]	number of graft units [d]
cage$_3$-GPCL	*s*-(PCL-NB)$_3$ ($M_{n,NMR}$ = 5,200)	5/1	0.10	30	26,200	42,900	1.20	8.3
		10/1	0.10	40	34,200	69,800	1.33	13.4
		20/1	0.20	90	58,800	118,000	1.21	22.7
		40/1	0.30	90	135,500	303,000	1.35	58.3
cage$_4$-GPCL	*s*-(PCL-NB)$_4$ ($M_{n,NMR}$ = 6,000)	3.75/1	0.20	90	24,000	40,200	1.27	6.7
		7.5/1	0.20	90	28,000	53,400	1.27	8.9
		15/1	0.30	150	44,400	95,200	1.30	15.9

[a] Polymerization conditions: temperature, r.t.; atmosphere, Ar; solvent, CH_2Cl_2. [b] Determined by SEC in tetrahydrofuran (THF) using PSt as the standard. [c] Determined by triple-detection SEC equipped with multiangle light scattering, viscosity, and refractive index detectors (SEC-MALS-Visco) in THF. [d] The number of cage repeating units in the obtained GPCLs was estimated as ($M_{n,MALS}$ of GPCL)/($M_{n,NMR}$ of MM).

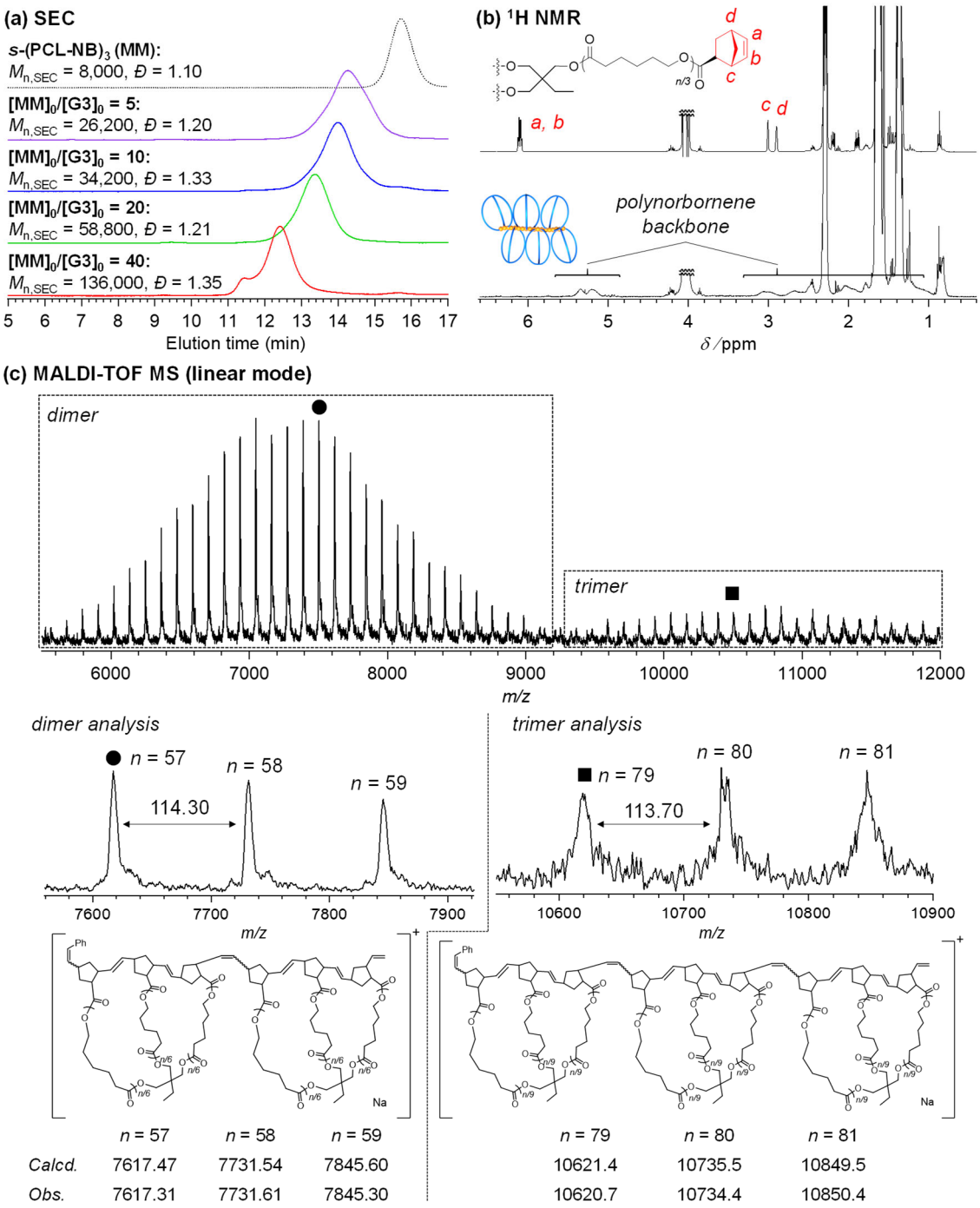

Figure 2. Structural analysis of graft polymers containing three-armed cage-shaped PCL side-chains (*cage*$_3$-GPCLs) prepared by cyclopolymerization using G3. (a) SEC traces of the three-armed star-shaped macromonomer (MM, namely *s*-(PCL-NB)$_3$; $M_{n,NMR}$ = 5,200 g mol^{-1}, $M_{n,SEC}$ = 8,000 g mol^{-1}, $Đ$ = 1.10; dotted line) and the *cage*$_3$-GPCLs obtained at [MM]$_0$/[G3]$_0$ = 5 (purple), 10 (blue), 20 (green), and 40 (red) in THF. The shoulder peak that appeared in the SEC traces of the product obtained at [MM]$_0$/[G3]$_0$ = 40 is due to the exclusion limit of the column (see Figure S4). (b) ^{1}H NMR spectra of *s*-(PCL-NB)$_3$ (upper) and *cage*$_3$-GPCL prepared at [MM]$_0$/[G3]$_0$ = 5 (lower) in $CDCl_3$ (400 MHz). (c)

matrix-assisted laser desorption/ionization-time of flight mass spectrometric analysis of *cage*$_3$-GPCL ($M_{n,SEC}$ = 12,000 g mol^{-1}, $Đ$ = 1.17).

To prove that the polymerization of the multifunctional macromonomer proceeded via the expected cyclopolymerization mechanism, the as-obtained product was characterized by SEC equipped with multiangle light scattering and viscosity detectors (SEC-MALS-Visco), ^{1}H NMR, and matrix-assisted laser desorption/ionization-time of flight mass spectrometry (MALDI-TOF MS). The absolute number-average molecular weight determined by SEC-MALS-Visco ($M_{n,MALS}$) in THF was 42900 g mol^{-1}, and the average number of repeating cage units was calculated to be 8.3, which is slightly higher than the theoretical value (5.0). In the ^{1}H NMR spectrum, the signals corresponding to the *exo*-norbornenyl group completely disappeared following the reaction, indicating that the ROMP proceeded quantitatively (Figure 1b). Combined with the fact that no multimerized product was found through SEC, this proves the absence of a dangling chain in the resulting GPCL. Although MALDI-TOF MS analysis can provide finer structural details, acquiring the spectrum from high-molecular-weight polymers is quite challenging. To overcome this difficulty, we separately prepared a low-molecular-weight sample ($M_{n,SEC}$ = 12000 g mol^{-1}, $Đ$ = 1.17) by cyclopolymerizing the macromonomer ($M_{n,NMR}$ = 4100 g mol^{-1}, $M_{n,SEC}$ = 6300 g mol^{-1}, $Đ$ = 1.05) at [*s*-(PCL-NB)$_3$]$_0$/[G3]$_0$ = 3. As shown in Figure 1c, the MALDI-TOF MS spectrum of the product exhibited a series of periodic

peaks having a regular interval of 114.30 Da, which is in good agreement with the mass of the ε-CL repeating unit. Crucially, we found two populations of molecular weight distribution, one of which was observed between the *m*/*z* values of 5000 and 9000 whereas the other was observed between the *m/z* values of 9000 and 12000. The peaks appearing in the lower molecular weight population were assigned to the desired GPCL containing two cage units; for example, the peak denoted by ● at *m*/*z* = 7617.31 closely matches the calculated mass for the dimer containing 57 ε-CL repeating units ($[M + Na]^+$ = 7617.47). In contrast, the peaks appearing in the higher molecular weight population were assigned to the GPCL containing three cage units; for example, the peak denoted by ■ at *m/z* = 10620.7 closely matches the calculated mass for the trimer containing 79 ε-CL repeating units ($[M + Na]^+$ = 10621.4). No peaks attributable to possible multiple G3 adducts (such as two G3 adducts; $[M + Na]^+$ = 7721.64, *n* = 57; Chart S1) were found, suggesting that the cyclopolymerization was initiated from a single G3 molecule to produce *cage*$_3$-GPCL possessing the expected chemical structure that lacks a dangling chain.

Since the cyclopolymerization of the trifunctional star-shaped macromonomer was performed in an accurately controlled manner to produce the desired *cage*-GPCL, the number of norbornenyl units in the polynorbornene backbone is expected to be an integral multiple of three. Based on this hypothesis, we envisioned that MALDI-TOF MS analysis of the polynorbornene backbone would provide direct proof of the expected cyclopolymerization mechanism. Accordingly, the *cage*$_3$-GPCL ($M_{n,SEC}$ = 28,600 g mol^{-1}, $Đ$ = 1.16; prepared by cyclopolymerization at [*s*-(PCL-NB)$_3$]$_0$/[G3]$_0$ = 10) was

subjected to methanolysis using sodium methoxide to selectively remove the PCL side-chain (see SI for the synthetic details). The MALDI-TOF MS spectrum of the methanolysis product exhibited a series of peaks that were assigned to poly(methyl norbornenecarboxylate)s consisting of 9, 12, 15, 18, and 21 repeating units (Figure S3). In addition, its regular peak interval (455.31 Da) was consistent with a trimer composed of methyl norbornenecarboxylate as the repeating unit (calculated mass = 456.25 Da). This result strongly supported the hypothesis that the desired *cage*-GPCL was precisely synthesized through a controlled cyclopolymerization in which intramolecular cyclization proceeded preferentially over intermolecular propagation. Overall, these structural characterizations confirm that star-shaped macromonomers are cyclopolymerized to produce GPCLs having cage-shaped topological side-chains (i.e., *cage*$_3$-GPCL).

One might expect that the undesired reactions could occur to produce the uncyclized by-products during the cyclopolymerization of *s*-(PCL-NB)$_3$, as shown in Figure S5a. However, our detailed structural characterization of the *cage*$_3$-GPs suggested that such undesired reactions hardly occur. First of all, ^{1}H NMR of the products confirmed no unreacted norbornenyl group. Given that the by-products (i) – (iii) with dangling chains (Figure S5a) must possess unreacted norbornenyl groups, the ^{1}H NMR results can exclude the occurrence of those by-products. Moreover, MALDI-TOF MS analysis of *cage*$_3$-GP shown in Figure 2 revealed that all the peaks were assignable to the expected chemical structures with the different number of PCL units. The by-products (iii) – (v) in Figure S5a are produced only when two or more G3 additions occurred. Since such multiple adducts possess one or

more extra G3-derived benzylidene units, those by-products can be distinguished from *cage*$_3$-GP by MALDI-TOF MS (Figure S5b,c). As mentioned before, no peak corresponding to such by-products was found in the spectra, confirming their negligibly small population. Another important evidence of successful cyclopolymerization is that no gelation occurred during the cyclopolymerizations. Given that the dangling chains exist in the products, this causes gelation through intermolecular propagation. No gelation occurred strongly supports that virtually no dangling chain formed and all the norbornenyl groups consumed for the cyclic repeating unit formations. These solid pieces of evidence proved that the cyclopolymerization of *s*-(PCL-NB)$_3$ produces the corresponding well-defined *cage*$_3$-GPs.

It has been reported that even a trace amount (˜0.1 wt%) of the linear contaminant in cyclic polymer affects the morphological and rheological properties.[32] Therefore, well-defined and highly pure samples are essential to accurately establish the structure-properties relationships. In this regard, our characterization demonstrated the well-controlled synthesis of *cage*-GPs; however, detecting such a small population of structural defects and impurities is challenging. While an in-depth analysis of possible structural defects in the *cage*-GPs is outside the scope of this study, cutting-edge separation methods (such as liquid chromatography at critical conditions and temperature gradient interaction chromatography)[33,34] could facilitate not only quantifying the multicyclic polymer purity but also removing possible by-products.

To further examine the controllability of the side-chain topology (i.e., *cage*$_4$-GPCL), the four-armed star-shaped macromonomer (*s*-(PCL-NB)$_4$; $M_{n,NMR}$ = 6000 g mol^{-1}, $M_{n,SEC}$ = 9900 g mol^{-1}, $Đ$ = 1.05)

was subjected to cyclopolymerization (Scheme 1b). For a reasonable comparison to the *cage*$_3$-GPCLs, the molecular weight of the PCL arm of *s*-(PCL-NB)$_4$ was fixed at ~1500 g mol^{-1}. Note that the perfect functionality of end-norbornenyl group in the *s*-(PCL-NB)$_4$ was also confirmed by ^{1}H NMR in similar manner as *s*-(PCL-NB)$_3$ (Figure S6). Under the established conditions, the cyclopolymerization of *s*-(PCL-NB)$_4$ ([*s*-(PCL-NB)$_3$]$_0$/[G3]$_0$ = 3.75/1) yielded a soluble product, demonstrating that the undesired intermolecular crosslinking was sufficiently suppressed even with the tetrafunctional macromonomer (Table 1). Indeed, the SEC trace of the product clearly shifted to a higher molecular region ($M_{n,SEC}$ = 24000 g mol^{-1}, $Đ$ = 1.27) compared to that of *s*-(PCL-NB)$_4$ ($M_{n,SEC}$ = 9900 g mol^{-1}, $Đ$ = 1.05), while retaining the monomodal peak (Figure S7). Furthermore, the ^{1}H NMR analysis of the product revealed the quantitative consumption of the norbornenyl groups (Figure S8). The number of four-armed cage-shaped units was determined to be 6.7 from its $M_{n,MALS}$. These results support that this synthetic strategy can be applied to tetrafuctional macromonomers to produce *cage*$_4$-GPCLs containing four-armed cage-shaped side-chains.

The established cyclopolymerization system permitted reliable control over the total molecular weight of *cage*$_3$- and *cage*$_4$-GPCLs in the range of ca. 40200–303000 g mol^{-1} in $M_{n,MALS}$ by varying the [macromonomer]$_0$/[G3]$_0$ ratio (Table 1). Although the cyclopolymerizations performed at elevated values of [macromonomer]$_0$/[G3]$_0$ (i.e., [*s*-(PCL-NB)$_3$]$_0$/[G3]$_0$ = 20) did not complete at [macromonomer]$_0$ = 0.10 mM, dosing slightly higher concentrations ([macromonomer]$_0$ = 0.20–0.30

mM) permitted quantitative polymerization. The maximum number of cage-shaped units was 58.3, which was obtained at [*s*-(PCL-NB)$_3$]$_0$/[G3]$_0$ = 40/1.

Kinetic study. To gain mechanistic insights into the cyclopolymerization of star-shaped macromonomers, we performed a kinetic study by monitoring the macromonomer conversion using SEC. With this objective, we investigated the (cyclo)polymerizations of not only *s*-(PCL-NB)$_3$ and *s*-(PCL-NB)$_4$, but also those of monofunctional (PCL-NB; $M_{n,NMR}$ = 2040 g mol^{-1}, $M_{n,SEC}$ = 2970 g mol^{-1}, $Đ$ = 1.12) and bifunctional (NB-PCL-NB; $M_{n,NMR}$ = 3200 g mol^{-1}, $M_{n,SEC}$ = 5600 g mol^{-1}, $Đ$ = 1.08) macromonomers to comprehensively understand the arm-number-dependent polymerization properties. The molecular weight of each macromonomer was fixed at ~1500 g mol^{-1} to ensure a fair comparison. The (cyclo)polymerization of each macromonomer was conducted at [norbornenyl group]$_0$/[G3]$_0$ = 15/1 (i.e., [NB-PCL-NB]$_0$/[G3]$_0$ = 7.5/1, [*s*-(PCL-NB)$_3$]$_0$/[G3]$_0$ = 5/1, and [*s*-(PCL-NB)$_4$]$_0$/[G3]$_0$ = 3.75/1) at [macromonomer]$_0$ = 0.2 mM. As shown in Figure 3a, the time-conversion plots showed that *s*-(PCL-NB)$_3$ reached complete conversion in 10 min (red plots), whereas complete conversion was observed at 30–50 min for PCL-NB and NB-PCL-NB (black and blue plots, respectively). The cyclopolymerization of *s*-(PCL-NB)$_4$ proved to be the quickest (~8 min, green plots) among the four macromonomers. These polymerizations followed first-order kinetics, exhibiting a distinctive feature of living/controlled polymerizations (Figure 3b). More importantly, the observed trend clearly indicates that the rate of cyclopolymerization increases with decreasing number of

intermolecular propagation reactions. Once the propagating chain-end (or G3 initiator) reacts to the macromonomer, the intramolecular consecutive cyclization takes place significantly more rapidly than intermolecular propagation. Therefore, intermolecular propagation is the rate-determining step of the cyclopolymerization. The cyclopolymerization mechanism is illustrated in Figure 3c. The initiating step involves the addition of G3 to the norbornenyl group on the macromonomer followed by the rapid intramolecular consecutive cyclization that forms a cage-shaped unit bearing an active Ru carbene. Due to the high dilution, the addition of the active Ru carbene to the adjacent macromonomer occurs quite slowly compared to the intramolecular reaction. Therefore, possible side reactions, such as the addition of multiple G3 molecules, dangling chain formation, and crosslinking reactions, are strongly suppressed, thereby producing well-defined *cage*-GPCLs.

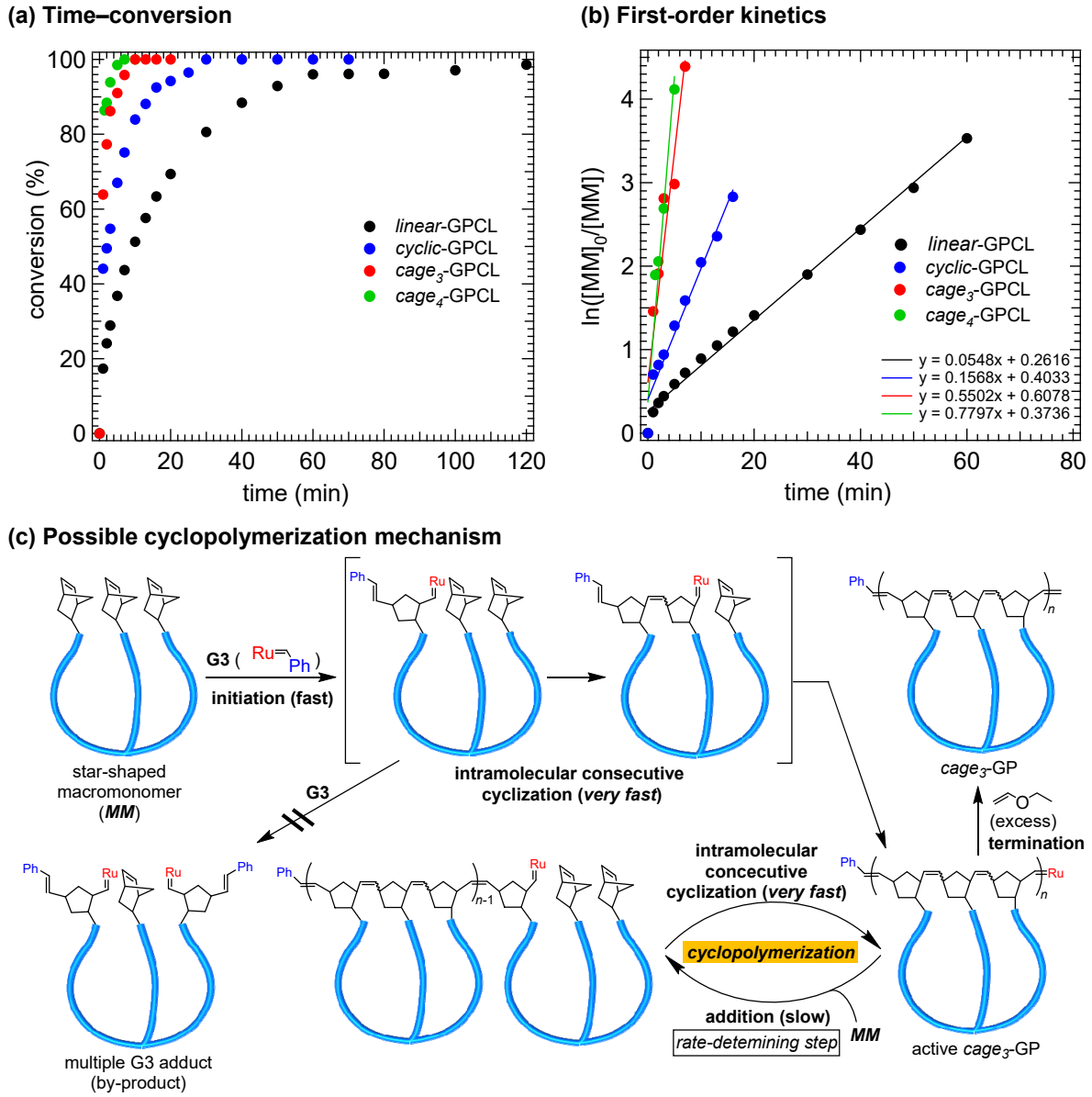

Figure 3. (a,b) Kinetic analyses of the (cyclo)polymerizations of PCL-NB, NB-PCL-NB, *s*-(PCL-NB)$_3$, and *s*-(PCL-NB)$_4$ ([PCL-NB]$_0$/[G3]$_0$ = 15/1; [NB-PCL-NB]$_0$/[G3]$_0$ = 7.5/1; [*s*-(PCL-NB)$_3$]$_0$/[G3]$_0$ = 5/1; [*s*-(PCL-NB)$_4$]$_0$/[G3]$_0$ = 3.75/1; [MM]$_0$ = 0.2 mM). (c) Proposed mechanism for the cyclopolymerization of three-armed star-shaped macromonomers to produce a well-defined *cage*$_3$-GPCL under a diluted condition.

Range of applicability to macromonomers. Thereafter, we applied this strategy to diverse polymer species to confirm its synthetic versatility. We performed the cyclopolymerization of a variety of

norbornenyl-end-functionalized star-shaped macromonomers, such as three- and four-armed star-shaped poly(L-lactide)s (*s*-(PLLA-NB)$_3$ and *s*-(PLLA-NB)$_4$, respectively), three-armed star-shaped poly(trimethylene carbonate) (*s*-(PTMC-NB)$_3$), and four-armed star-shaped poly(ethylene glycol) (*s*-(PEG-NB)$_4$) having a $M_{n,NMR}$ of 6000–8000 g mol^{-1}, to obtain the corresponding GPCLs (*cage$_x$*-GPLLA (x = 3 and 4), *cage$_3$*-GPTMC, and *cage$_4$*-GPEG, respectively; see Scheme 2 and Table S1). Specifically, the PLLA and PTMC macromonomers were prepared by the ring-opening polymerizations of L-lactide and trimethylene carbonate, respectively, using triol or tetraol initiator and tin(II) 2-ethylhexanoate and diphenyl phosphate catalysts,[30,35] followed by end-functionalization with norbornenyl carboxylic acid. Similarly, the PEG macromonomer was obtained by appending a norbornenyl group to each terminus of a commercially available four-armed star-shaped PEG. The cyclopolymerization proceeded successfully for all the macromonomers and yielded soluble products under the optimized conditions ([*s*-(PLLA-NB)$_3$]$_0$/[G3]$_0$ = 10/1 and [*s*-(PLLA-NB)$_3$]$_0$ = 0.2 mM; [*s*-(PLLA-NB)$_4$]$_0$/[G3]$_0$ = 7.5/1 and [*s*-(PLLA-NB)$_4$]$_0$ = 0.2 mM; [*s*-(PTMC-NB)$_3$]$_0$/[G3]$_0$ = 10/1 and [*s*-(PTMC-NB)$_3$]$_0$ = 0.075 mM; [*s*-(PEG-NB)$_4$]$_0$/[G3]$_0$ = 7.5/1 and [*s*-(PEG-NB)$_4$]$_0$ = 0.1 mM). While the SEC analysis revealed that the products exhibited small shoulder peaks in the higher molecular region, the major peak attested to increased molecular weights (16600–38500 in $M_{n,SEC}$) with respect to the corresponding macromonomer, and had narrow $Đ$ values (1.15–1.45) (Figures S9–12; also find their ^{1}H NMR spectra in Figures S13–16). Therefore, the presented strategy is applicable to a wide range of macromonomers for producing GPs from different polymer species.

Scheme 2. Range of applicability to macromonomers. Cyclopolymerizations of (a,b) three- and four-armed star-shaped PLLA, (c) PTMC, and (d) PEG macromonomers to yield *cage*$_3$-GPLLA, *cage*$_4$-GPLLA, *cage*$_3$-GPTMC, and *cage*$_4$-GPEG, respectively

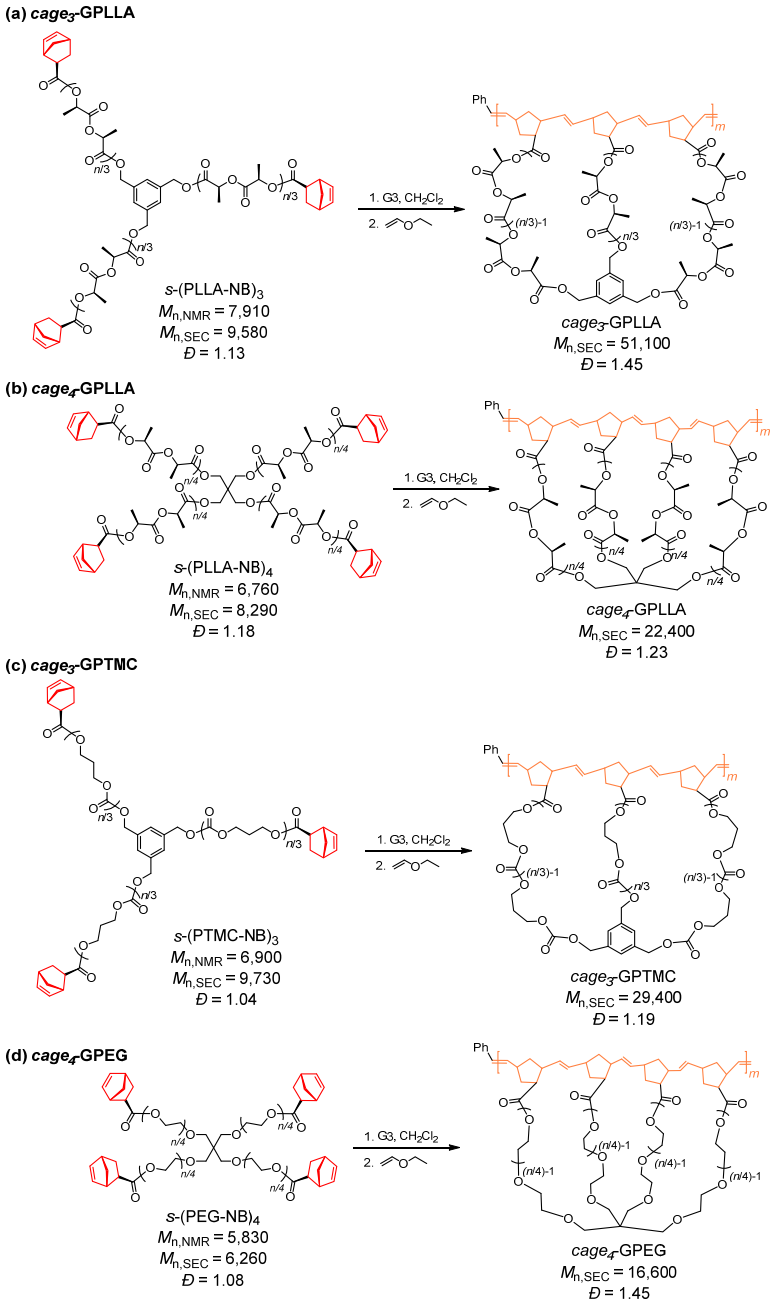

Structure-property relationships of *cage*-GPCLs and their linear and monocyclic counterparts.

It is of fundamental interest to systematically investigate how the topology of the side-chain affects the physical properties of topological GPCLs in bulk and solution states, which could facilitate topology-directed material design. Therefore, we initially evaluated the equilibrium melting temperature ($T_m°$) using differential scanning calorimetry (DSC). A series of linear- and cyclic-chain-grafted GPCLs (*l*-GPCLs and *c*-GPCLs, respectively) as well as monomeric cyclic and cage-shaped PCL units (PCL-NB, *c*-PCL, *cage*$_3$-PCL, and *cage*$_4$-PCL; Chart 1) were also prepared and subjected to DSC analyses (see Table 2 and Figures S17–21). Because $T_m°$ is defined as the estimated melting temperature of an infinite stack of extended chain crystals, it should provide objective and extensive insight into the crystallization properties while excluding the potential effects of the crystallization kinetics on T_m (i.e., the dependence of T_m on thermal history).[36,37] The $T_m°$ value of each GPCL was determined by the linear Hoffman–Weeks extrapolation method,[36] wherein the T_m values for the isothermally crystallized samples were plotted against the crystallization temperatures (T_cs), and their linear extrapolation to the line of $T_m = T_c$ gave $T_m°$ as the intersection (see DSC experimental in SI for details). Note that a series of GPCLs used in the analysis had $M_{n,MALS}$ values of 42900–55600 g mol^{-1}. The Hoffman–Weeks plots of the topological GPCLs shown in Figure 4a revealed a unique trend of $T_m°$ as follows: *l*-GPCL (60.6 °C) ≈ *cage*$_3$-GPCL (60.3 °C) > *c*-GPCL (56.8 °C) > *cage*$_4$-GPCL (51.8 °C). Notably, this trend is different from that of the monomeric cyclic and cage-shaped PCL units; $T_m°$ of PCL-NB, *c*-PCL, *cage*$_3$-PCL, and *cage*$_4$-PCL were similarly estimated to be 59.7, 65.0,

61.3, and 60.1 °C, respectively (see Table 2). Specifically, the highest $T_m°$ was calculated for *cage*$_3$-GPCL among the cyclic/cage-shaped GPCLs and for *c*-PCL among the monomeric cyclic/cage-shaped PCLs. The dense grafting of the cyclic/cage-shaped side-chain units could cause a discrepancy in the topology-dependent trend of $T_m°$ between the monomeric cyclic/cage-shaped PCLs and GPCLs. For the cage-shaped PCLs and GPCLs, the side-chain segments around the branched points should possess lower chain mobility and be difficult to crystallize. The side-chain segments farther from the branched points should possess higher chain mobility and crystallize readily. In the case of cage-shaped GPCLs, the spatial interrelation between the neighboring cage-shaped units is determined by their junction with the polynorbornene backbone. When the side-chain segments in the cage-shaped GPCLs crystallize into the lamellar crystal, such steric constraints hinder crystallization in terms of chain mobility. However, the "fixed" spatial interrelation of the neighboring grafted cages should favor chain diffusion to the growth front of lamellar crystals. In the case of *cage*$_3$-GPCL, the side-chain segments in the same cage and perhaps neighboring segments should be located at distances and with orientations that are suitable for chain packing, resulting in an increased $T_m°$. However, further increase in the number of arms of the topological side-chain unit causes steric hindrance around the polynorbornene backbone and four-branched pentaerythritol residue,[38] which could interfere with the crystallization due to the significantly reduced chain mobility, resulting in a much lower $T_m°$ for *cage*$_4$-GPCL than for *cage*$_3$-GPCL. To gain further insight into the crystallization behavior and crystalline hierarchical structure, wide-angle X-ray diffraction (WAXD) and small-angle X-ray scattering (SAXS) experiments (Table

S2, Figures S22 and S23) were performed on isothermally crystallized topological GPCLs ($M_{n,MALS}$ = 33200–42900 g mol^{-1}, crystallized at 30 °C for 48 h). As shown in Figure S23, each WAXD profile exhibited diffraction peaks corresponding to the (110) and (200) planes of the PCL crystal.[39,40] Similar to the cyclic/cage-shaped PCLs,[31] no significant change was observed in the positions of the diffraction peaks upon varying the side-chain topology, confirming that the side-chain topology does not affect the crystallographic unit cell (i.e., chain conformation and packing). This result can be interpreted as the side-chain segments being sufficiently separated from the branched points in topological GPCLs and PCLs crystallize in an identical conformation and packing to that of the linear PCL, whereas those around the branched points do not crystallize inherently. Correlation function analysis of the SAXS profiles (Figure S24) revealed the thicknesses of the crystalline lamellae (l_c) and the amorphous layer (l_a), and the long period ($L_p = l_c + l_a$). Interestingly, topological GPCLs retained a constant l_c value (4.4–4.5 nm), while the monomeric cyclic/cage-shaped PCLs exhibited an increasing trend in the l_c values from 3.2 to 4.5 nm with increase in the number of arms. The cage-shaped PCLs (*cage*$_3$-PCL and *cage*$_4$-PCL) possessed comparable values of l_c (~4.5 nm), l_a (~7.0 nm), and L_p (11.5 nm). In contrast, *cage*$_4$-GPCL possessed a longer l_a (9.4 nm) than *cage*$_3$-GPCL (7.5 nm), albeit possessing an identical l_c (4.5 nm). The crystallinity obtained from WAXD (X_{WAXD}) as well as the ratio of l_c and L_p (l_c/L_p), which is a measure of crystallinity, decreased with increasing number of arms of the cage-shaped GPCLs. In addition, the X_{WAXD} and l_c/L_p for *cage*$_3$-GPCL were comparable to those for *cage*$_3$-PCL, whereas *cage*$_4$-GPCL possessed lower X_{WAXD} and l_c/L_p compared to *cage*$_4$-PCL. These trends

are consistent with the magnitude relation in $T_m°$, supporting the dense-grafting effect and the higher crystallizability of *cage*$_3$-GPCL than that of *cage*$_4$-GPCL.

Chart 1. List of topological counterparts used for systematic characterization. Linear and cyclic GPCLs (*l*-GPCL and *c*-GPCL) and monomeric PCLs (PCL-NB, *c*-PCL, *cage*$_3$-PCL, and *cage*$_4$-PCL)

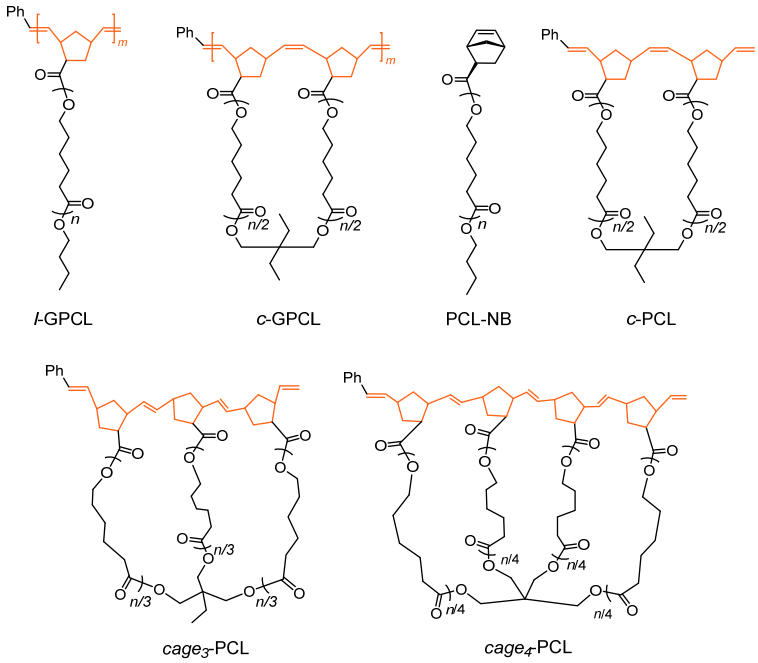

Table 2. Physical properties of GPCLs having various topological side-chains and their corresponding monomeric cyclic and cage-shaped PCLs

sample	Number of side-chain units [a]	$M_{n,MALS}$ [b] (g mol^{-1})	$M_{w,MALS}$ [b] (g mol^{-1})	$Đ$ [c]	T_m° (°C)	D_h [b] (nm)	$[\eta]$ [b] (mL g^{-1})
l-GPCL	10.4	33,200	33,500	1.06	-[d]	9.0	16.8
	16.7	52,600	53,700	1.08	60.6	10.8	18.4
	36.8	118,000	118,000	1.11	-[d]	15.4	24.4
c-GPCL	10.7	34,300	35,100	1.14	-[d]	8.4	13.2
	17.4	55,600	56,200	1.12	56.8	10.2	14.8
	21.6	69,200	69,700	1.15	-[d]	11.2	16.0
cage$_3$-GPCL	8.3	42,900	45,700	1.19	60.3	9.2	14.0
	13.4	69,800	78,700	1.33	60.5	11.4	15.6
	22.7	118,000	122,000	1.21	60.9	14	18.1
	58.3	303,000	319,000	1.35	61.5	22.8	29.4
cage$_4$-GPCL	6.7	40,200	45,400	1.27	-[d]	8.8	12.2
	8.9	53,400	57,400	1.27	51.8	9.6	12.7
	15.9	95,200	105,000	1.30	-[d]	12.8	15.9
PCL-NB	-	1,610	1,820	1.12	59.7	2.6	8.8
c-PCL	-	3,130	3,470	1.08	65.0	3.0	6.7
cage$_3$-PCL	-	3,960	4,090	1.05	61.3	3.2	6.4
cage$_4$-PCL	-	5,550	5,600	1.05	60.1	3.6	7.0

[a] Number of linear, cyclic, or cage-shaped repeating units in the as-obtained GPCLs estimated from ($M_{n,MALS}$ of GPCL)/($M_{n,NMR}$ of MM). [b] Determined using SEC-MALS-Visco in THF. [c] Determined by SEC in THF using PSt as the standard. [d] Not determined.

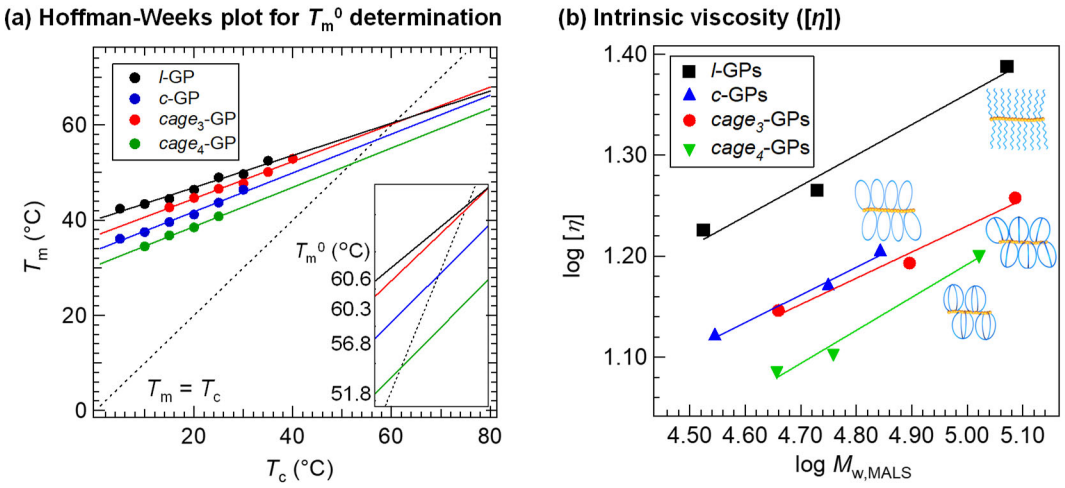

Figure 4. Structure-property relationships of topological GPCLs and their counterparts. (a) Hoffman-Weeks plot of GPCLs. The inset contains a magnification of the plot around the point of intersection, which represents the $T_m°$ value of each GPCL. (b) Double-logarithmic plots of $M_{w,MALS}$ versus [η] for *l*-GPCLs (black), *c*-GPCLs (blue), *cage*$_3$-GPCLs (red), and *cage*$_4$-GPCLs (green) (in THF).

Thereafter, we evaluated the solution properties, such as intrinsic viscosity ([η]) and hydrodynamic diameter (D_h), using SEC-MALS-Visco in THF. As shown in Figure 4b, [η] values of cage-type GPCLs (*cage*$_3$-GPCLs and *cage*$_4$-GPCLs; 12.2–18.1 mL g^{-1}) were found to be smaller than those of their linear and cyclic-type counterparts (13.2–24.4 mL g^{-1}). Specifically, the [η] values decreased in the following order: *l*-GPCLs > *c*-GPCLs > *cage*$_3$-GPCLs > *cage*$_4$-GPCLs. This decreasing trend in [η] with increasing number of arms is consistent with that of the monomeric cyclic/cage-shaped PCLs ([η] = 8.8, 6.7, 6.4, and 7.0 mL g^{-1} for PCL-NB, *c*-PCL, *cage*$_3$-PCL, and *cage*$_4$-PCL, respectively; See Table 2). While a series of monomeric PCLs appeared to have no correlation between the topology and D_h values, the D_h values of GPCLs decreased with increases in the number of arms of a repeating side-chain unit when compared between the samples possessing comparable total molecular weights

(see Figure S25). These results confirmed that the cage-shaped topological side-chain endows the graft polymers with reduced overall chain dimensions, significantly fewer chain entanglements, and greater side-chain density.[41–43] Such unique properties can be attractive advantages of cage-type topological GPs over cyclic GPs for applications in lubricating and antifouling coatings.

Conclusions

In this study, we successfully demonstrated the cyclopolymerization of norbornenyl-end-functionalized star-shaped macromonomers to produce well-defined topological GPCLs possessing cage-shaped side-chains with tunable numbers of arms and cage units. The mechanistic investigation revealed that the presented cyclopolymerization proceeds in an accurately controlled manner, which is composed of the repetition of rapid intramolecular consecutive cyclization and subsequent rate-determining intermolecular addition reaction. The established cyclopolymerization system was found to be applicable to diverse macromonomers, including PLLA, PTMC, and PEG. Furthermore, we systematically characterized a series of GPCLs with varying molecular weights and side-chain topologies, which revealed that the cage-shaped side-chain topologies significantly affected the crystallization behavior, hydrodynamic diameter, and viscosity. Overall, the simple yet robust cyclopolymerization method enabled, for the first time, the synthesis of well-defined topological graft polymers carrying controllable cage-shaped side-chains, which are difficult to obtain using conventional graft polymer synthetic approaches. Because of the structural tunability of the polymer

backbone, side-chain topology, and degree of polymerization (i.e., the number of side-chain units) of the topological GPs, the topology-directed molecular design of functional materials, such as surface modifiers, should be achieved. By taking advantage of the controlled/living nature of the cyclopolymerization presented herein, we are currently working on synthesizing chain-end- and side-chain-functionalized topological GPs to create high-performance surface coating materials.

ASSOCIATED CONTENT

Supporting Information

Experimental details and additional data (^{1}H NMR, MALDI-TOF MS, SEC, DSC, SAXS, WAXD) (PDF). Supporting Information is available free of charge on the ACS Publications website.

AUTHOR INFORMATION

Corresponding Authors

*Email: isono@eng.hokudai.ac.jp (T.I.)

*Email: satoh@eng.hokudai.ac.jp (T.S.)

Author Contributions

The manuscript was written through contributions of all authors. All authors have given approval to the final version of the manuscript.

Funding Sources

This work was financially supported by the MEXT Grant-in-Aid for Challenging Exploratory Research (19K22209), Grant-in-Aid for Scientific Research (A and B) (19H00905 and 19H02769), Grant-in-Aid for Scientific Research on Innovative Areas “Hybrid Catalysis” (18H04639 and 20H04798), JST CREST (Grant Number JPMJCR19T4), Photo-excitonix Project (Hokkaido University), and the Creative Research Institute (CRIS, Hokkaido University). Y. M. was funded by a JSPS Fellowship for Young Scientists.

Notes

The authors declare no competing financial interests.

ACKNOWLEDGMENT

This work was performed with the approval of the Photon Factory Program Advisory Committee (Proposal and 2019G579 and 2020G649).

References

(1) Polymeropoulos, G.; Zapsas, G.; Ntetsikas, K.; Bilalis, P.; Gnanou, Y.; Hadjichristidis, N. *50th Anniversary Perspective* : Polymers with Complex Architectures. *Macromolecules* **2017**, *50*, 1253–1290.

(2) Clarson, S. J.; Semlyen, J. A. Cyclic Polysiloxanes: 1. Preparation and Characterization of Poly(Phenylmethylsiloxane). *Polymer* **1986**, *27*, 1633–1636.

(3) Zimm, B. H.; Stockmayer, W. H. The Dimensions of Chain Molecules Containing Branches and Rings. *J. Chem. Phys.* **1949**, *17*, 1301–1314.

(4) Zhu, X.; Zhou, N.; Zhang, Z.; Sun, B.; Yang, Y.; Zhu, J.; Zhu, X. Cyclic Polymers with Pendent Carbazole Units: Enhanced Fluorescence and Redox Behavior. *Angew. Chemie* **2011**, *123*, 6745–6748.

(5) Pipertzis, A.; Hossain, M. D.; Monteiro, M. J.; Floudas, G. Segmental Dynamics in Multicyclic Polystyrenes. *Macromolecules* **2018**, *51*, 1488–1497.

(6) Hossain, M. D.; Reid, J. C.; Lu, D.; Jia, Z.; Searles, D. J.; Monteiro, M. J. Influence of Constraints within a Cyclic Polymer on Solution Properties. *Biomacromolecules* **2018**, *19*, 616–625.

(7) Yamamoto, T.; Tezuka, Y. Topological Polymer Chemistry: A Cyclic Approach toward Novel Polymer Properties and Functions. *Polym. Chem.* **2011**, *2*, 1930–1941.

(8) Uehara, E.; Deguchi, T. Mean-Square Radius of Gyration and the Hydrodynamic Radius for Topological Polymers Expressed with Graphs Evaluated by the Method of Quaternions Revisited. *React. Funct. Polym.* **2018**, *133*, 93–102.

(9) Zhang, K.; Lackey, M. A.; Cui, J.; Tew, G. N. Gels Based on Cyclic Polymers. *J. Am. Chem. Soc.* **2011**, *133*, 4140–4148.

(10) Honda, S.; Yamamoto, T.; Tezuka, Y. Topology-Directed Control on Thermal Stability: Micelles Formed from Linear and Cyclized Amphiphilic Block Copolymers. *J. Am. Chem. Soc.* **2010**, *132*, 10251–10253.

(11) Liu, W.; Dong, Y.; Liu, S.; Wei, T.; Wu, Z.; Chen, H. Enhancement of Bactericidal Activity via Cyclic Poly(Cationic Liquid) Brushes. *Macromol. Rapid Commun.* **2019**, *40*, 1–6.

(12) Wei, T.; Zhou, Y.; Zhan, W.; Zhang, Z.; Zhu, X.; Yu, Q.; Chen, H. Effects of Polymer Topology on Biointeractions of Polymer Brushes: Comparison of Cyclic and Linear Polymers. *Colloids Surfaces B Biointerfaces* **2017**, *159*, 527–532.

(13) Sakurai, S.; Watanabe, H.; Takahara, A. Preparation and Characterization of Looped Polydimethylsiloxane Brushes. *Polym. J.* **2014**, *46*, 117–122.

(14) Trachsel, L.; Romio, M.; Grob, B.; Zenobi-Wong, M.; Spencer, N. D.; Ramakrishna, S. N.; Benetti, E. M. Functional Nanoassemblies of Cyclic Polymers Show Amplified Responsiveness and Enhanced Protein-Binding Ability. *ACS Nano* **2020**, *14*, 10054–10067.

(15) Morgese, G.; Trachsel, L.; Romio, M.; Divandari, M.; Ramakrishna, S. N.; Benetti, E. M. Topological Polymer Chemistry Enters Surface Science: Linear versus Cyclic Polymer Brushes. *Angew. Chem. Int. Ed.* **2016**, *55*, 15583–15588.

(16) Wang, Y.; Quinsaat, J. E. Q.; Ono, T.; Maeki, M.; Tokeshi, M.; Isono, T.; Tajima, K.; Satoh, T.; Sato, S. ichiro; Miura, Y.; Yamamoto, T. Enhanced Dispersion Stability of Gold Nanoparticles by the Physisorption of Cyclic Poly(Ethylene Glycol). *Nat. Commun.* **2020**, *11*, 6089.

(17) Morgese, G.; Cavalli, E.; Rosenboom, J. G.; Zenobi-Wong, M.; Benetti, E. M. Cyclic Polymer Grafts That Lubricate and Protect Damaged Cartilage. *Angew. Chem. Int. Ed.* **2018**, *57*, 1621–1626.

(18) Morgese, G.; Cavalli, E.; Müller, M.; Zenobi-Wong, M.; Benetti, E. M. Nanoassemblies of Tissue-Reactive, Polyoxazoline Graft-Copolymers Restore the Lubrication Properties of Degraded Cartilage. *ACS Nano* **2017**, *11*, 2794–2804.

(19) Ramakrishna, S. N.; Morgese, G.; Zenobi-Wong, M.; Benetti, E. M. Comblike Polymers with Topologically Different Side Chains for Surface Modification: Assembly Process and Interfacial Physicochemical Properties. *Macromolecules* **2019**, *52*, 1632–1641.

(20) Lehn, J. M. Cryptates: Inclusion Complexes of Macropolycyclic Receptor Molecules. *Pure Appl. Chem.* **1978**, *50*, 871–892.

(21) Sheiko, S. S.; Sumerlin, B. S.; Matyjaszewski, K. Cylindrical Molecular Brushes: Synthesis, Characterization, and Properties. *Prog. Polym. Sci.* **2008**, *33*, 759–785.

(22) Gavrilov, M.; Amir, F.; Kulis, J.; Hossain, M. D.; Jia, Z.; Monteiro, M. J. Densely Packed Multicyclic Polymers. *ACS Macro Lett.* **2017**, *6*, 1036–1041.

(23) Liu, C.; Fei, Y. Y.; Zhang, H. L.; Pan, C. Y.; Hong, C. Y. Effective Construction of Hyperbranched Multicyclic Polymer by Combination of ATRP, UV-Induced Cyclization, and Self-Accelerating Click Reaction. *Macromolecules* **2019**, *52*, 176–184.

(24) Amir, F.; Hossain, M. D.; Jia, Z.; Monteiro, M. J. Precise Grafting of Macrocyclics and Dendrons to a Linear Polymer Chain. *Polym. Chem.* **2016**, *7*, 6598–6607.

(25) Isono, T.; Sasamori, T.; Honda, K.; Mato, Y.; Yamamoto, T.; Tajima, K.; Satoh, T. Multicyclic Polymer Synthesis through Controlled/Living Cyclopolymerization of α,ω-Dinorbornenyl-Functionalized Macromonomers. *Macromolecules* **2018**, *51*, 3855–3864.

(26) Choi, T. L.; Grubbs, R. H. Controlled Living Ring-Opening-Metathesis Polymerization by a Fast-Initiating Ruthenium Catalyst. *Angew. Chem. Int. Ed.* **2003**, *42*, 1743–1746.

(27) Hibi, Y.; Ouchi, M.; Sawamoto, M. Sequence-Regulated Radical Polymerization with a Metal-Templated Monomer: Repetitive ABA Sequence by Double Cyclopolymerization. *Angew. Chem. Int. Ed.* **2011**, *50*, 7434–7437.

(28) Kang, C.; Park, H.; Lee, J. K.; Choi, T. L. Cascade Polymerization via Controlled Tandem Olefin Metathesis/Metallotropic 1,3-Shift Reactions for the Synthesis of Fully Conjugated Polyenynes. *J. Am. Chem. Soc.* **2017**, *139*, 11309–11312.

(29) Kakuchi, T.; Nonokawa, R.; Umeda, S.; Satoh, T.; Yokota, K. Ring-Opening and Ring-Forming Polymerization of 1,2:5,6:9,10-Triepoxydecane Leading to a Highly Regioselective Polymer Consisting of Octahydrobifuranyl Unit. *Macromolecules* **2000**, *33*, 246–247.

(30) Makiguchi, K.; Satoh, T.; Kakuchi, T. Diphenyl Phosphate as an Efficient Cationic Organocatalyst for Controlled/Living Ring-Opening Polymerization of δ-Valerolactone and ε-Caprolactone. *Macromolecules* **2011**, *44*, 1999–2005.

(31) Mato, Y.; Honda, K.; Tajima, K.; Yamamoto, T.; Isono, T.; Satoh, T. A Versatile Synthetic Strategy for Macromolecular Cages: Intramolecular Consecutive Cyclization of Star-Shaped Polymers. *Chem. Sci.* **2019**, 440–446.

(32) Kapnistos, M.; Lang, M.; Vlassopoulos, D.; Pyckhout-Hintzen, W.; Richter, D.; Cho, D.; Chang, T.; Rubinstein, M. Unexpected Power-Law Stress Relaxation of Entangled Ring Polymers. *Nat. Mater.* **2008**, *7*, 997–1002.

(33) Chang, T.; Lee, H. C.; Lee, W.; Park, S.; Ko, C. Polymer Characterization by Temperature Gradient Interaction Chromatography. *Macromol. Chem. Phys.* **1999**, *200*, 2188–2204.

(34) Ryu, J.; Chang, T. Thermodynamic Prediction of Polymer Retention in Temperature-Programmed HPLC. *Anal. Chem.* **2005**, *77*, 6347–6352.

(35) Gilding, D. K.; Reed, A. M. Biodegradable Polymers for Use in Surgery-Polyglycolic/Poly(Actic Acid) Homo- and Copolymers: 1. *Polymer* **1979**, *20*, 1459–1464.

(36) Hoffman, J. D.; Weeks, J. J. Melting Process and the Equilibrium Melting Temperature of Polychlorotrifluoroethylene. *J. Res. Natl. Bur. Stand. Sect. A Phys. Chem.* **1962**, *66A*, 13.

(37) Marand, H.; Xu, J.; Srinivas, S. Determination of the Equilibrium Melting Temperature of Polymer Crystals: Linear and Nonlinear Hoffman-Weeks Extrapolations. *Macromolecules* **1998**, *31*, 8219–8229.

(38) Ree, B. J.; Mato, Y.; Xiang, L.; Kim, J.; Isono, T.; Satoh, T. Topologically Controlled Phase Transitions and Nanoscale Film Self-Assemblies of Cage Poly(ε-Caprolactone) and Its Counterparts . *Polym. Chem.* **2021**, *12*, 744–758.

(39) Bittiger, H.; Marchessault, R. H.; Niegisch, W. D. Crystal Structure of Poly-ε-Caprolactone. *Acta Crystallogr. Sect. B Struct. Crystallogr. Cryst. Chem.* **1970**, *26*, 1923–1927.

(40) Chatani, Y.; Okita, Y.; Tadokoro, H.; Yamashita, Y. Structural Studies of Polyesters. III. Crystal Structure of Poly-ε-Caprolactone. *Polym. J.* **1970**, *1*, 555–562.

(41) Noda, T.; Doi, Y.; Ohta, Y.; Takata, S. ichi; Takano, A.; Matsushita, Y. Preparation, Characterization, and Dilute Solution Properties of Four-Branched Cage-Shaped Poly(Ethylene Oxide). *J. Polym. Sci.* **2020**, *58*, 2098–2107.

(42) Gauthier-Jaques, M.; Theato, P. Synergy of Macrocycles and Macromolecular Topologies: An Efficient [34]Triazolophane-Based Synthesis of Cage-Shaped Polymers. *ACS Macro Lett.* **2020**, *9*, 700–705.

(43) Oike, H.; Imaizumi, H.; Mouri, T.; Yoshioka, Y.; Uchibori, A.; Tezuka, Y. Designing Unusual Polymer Topologies by Electrostatic Self-Assembly and Covalent Fixation. *J. Am. Chem. Soc.* **2000**, *122*, 9592–9599.